J Eng Math
DOI 10.1007/s10665-009-9303-1

Waves due to an oscillating and translating disturbance in a two-layer density-stratified fluid

Mohammad-Reza Alam · Yuming Liu · Dick K. P. Yue

Received: 30 April 2008 / Accepted: 5 June 2009

Abstract Wave generation due to the steady translational motion of an oscillatory disturbance in a two-layer density-stratified fluid is studied. In the context of linearized two- and three-dimensional potential flow, explicit expressions for the Green functions are derived and limiting cases discussed. Of special interest are the waves in the far field. The number and amplitudes of these waves depend on the characteristics of the disturbance (location, speed and oscillation frequency) and the ocean (stratified layer density and depth ratios). These dependencies are elucidated in concrete examples. An interesting finding, for example, is that, for constant frequency, there are critical speeds (as functions of density and depth ratios) at which the specific amplitudes attain maxima. For the more general problem and as an independent validation, an efficient numerical scheme for the problem based on a spectral method is developed. Direct simulation results compare well with analytical predictions in the near- and far-fields and offer a powerful tool for practical problems with general time-dependent motions of one or more bodies.

Keywords Green function · Moving and oscillating disturbance · Spectral method · Two-layer fluid

1 Introduction

The linear problem of wave generation and propagation by a submerged disturbance, when it translates with a constant speed while its strength is sinusoidally oscillating in time, is considered analytically and numerically in a two-layer density-stratified fluid. Understanding of waves due to the motion of a submerged body has practical applications ranging from non-acoustic detection of underwater vehicles [1], to seakeeping and wave-load calculations on moored/floating offshore structures. In stratified waters, and particularly in littoral zones, it can help understand generation of internal gravity waves. In the inverse problem, density stratification hence ocean-body composition can be found from the wake pattern behind a moving object [2,3]. This work is motivated by the need for a better understanding of wakes of heavy ocean vehicles in strong stratified waters.

In a homogeneous fluid, the linear two-dimensional problem of far-field waves created by an oscillating and translating disturbance was studied in [4] (see also [5]), followed by others who included effects of nonlinearity and considered the asymptotic behaviors near the critical frequency (see e.g. [6–9]).

M.-R. Alam · Y. Liu · D. K. P. Yue (✉)
Department of Mechanical Engineering, Massachusetts Institute of Technology, Cambridge, MA, USA
e-mail: yue@mit.edu

Published online: 27 June 2009

For a two-layer density-stratified fluid, the steady flow past a submerged obstacle is well studied (see e.g. the monograph by Baines [10] where the rigid-lid assumption is used). In the presence of a free surface and deep lower layer, Voitsenya [11] derived the three-dimensional potential for a pulsating source and a vortex. For the same setup, Hudimac [12] showed that a moving ship generates an internal-wave system similar to the surface Kelvin waves. For speeds less than a critical speed, the internal ship wave consists of both transverse and divergent waves, while above that critical speed, only divergent waves persist [13,14].

For finite stratified layer depths, Yeung and Nguyen [15] obtained the Green function for a constant-strength source moving with steady speed in the upper layer. These results are extended, theoretically and experimentally, in [1] to a dipole located in the lower layer. For a disturbance near the interface of two deep-layer fluids (i.e., a system of two semi-infinite fluids), Lu and Chwang [16] derived analytical expressions for the three-dimensional interfacial waves due to a fundamental singularity.

The present work is motivated by the possibility of observing surface and internal disturbance associated with ships and submarines in strong stratified waters such as in warm littoral zones. We consider the general two- and three-dimensional problem of wave generation by an oscillatory source translating with steady forward speed in a two-layer density-stratified fluid. Depending on the Froude number and dimensionless frequency of the motion, and the ratios of depths and densities of the two layers, up to eight distinct far-field free waves can be obtained and for sufficiently small forward speed two of these can advance ahead of the source.

The formulation of the problem is given in Sect. 2, followed by a kinematic analysis based on the dispersion relation that provides the wavenumber and frequency of the far-field waves. To obtain the amplitudes of these waves and information in the near field, we solve the boundary-value problem for the Green function (Sect. 3) in two (Sect. 3.1, 3.3) and three dimensions (Appendix). The Green functions differ depending on whether the source is located in the upper (Sect. 3.1) or lower fluid (Sect. 3.3), and their dependencies on the physical parameters are discussed (Sect. 3.4). In the limit of deep fluid layers, the Green function simplifies substantially and each of the wave components can be worked out explicitly (Sect. 3.2). In Sect. 4, we develop an efficient numerical scheme for the general problem of possibly multiple disturbances with time-varying speeds and motion frequencies. The algorithm is the extension of a high-order spectral method originally developed to simulate nonlinear gravity wave–wave interactions in a single fluid layer [17]. The numerical method provides independent validation of the earlier analysis. This is performed in Sect. 4.2 for the near- and far-field waves.

2 Problem formulation

We consider a two-layer density-stratified fluid where the upper and lower fluid layers have, respectively, mean depths h_u and h_ℓ, and fluid densities ρ_u and ρ_ℓ (density ratio $\mathcal{R} \equiv \rho_u/\rho_\ell$). Hereafter, subscript u/ℓ denotes quantities associated with the upper/lower fluid layers. In a Cartesian coordinate system with the x, y-axes on the mean free surface and the z-axis positive upward, the two-layer fluid rests on a flat horizontal bottom $z = -h_u - h_\ell$ and has surface and interface elevations $\eta_u(x, y, t)$, and $\eta_\ell(x, y, t)$, respectively.

We consider a point source with pulsating strength $m = m_0 \cos\omega_0 t$, moving with forward speed U in the x-direction, located at a fixed (mean) depth $z = z_0$. We assume that the fluids in both layers are homogeneous, incompressible, immiscible and inviscid so that the fluid motion is irrotational. The effect of surface tension is neglected. The flow in each layer is described by a velocity potential, $\phi_u(x, y, z, t)$ and $\phi_\ell(x, y, z, t)$. In a stationary frame of reference the linearized governing equations are:

$$\nabla^2\phi_u = m_0\,\delta(x - x_0 - Ut, 0, z - z_0)\cos\omega_0 t, \quad -h_u < z < 0, \tag{2.1a}$$

$$\nabla^2\phi_\ell = 0, \quad -h_u - h_\ell < z < -h_u, \tag{2.1b}$$

$$\eta_{u,t} = \phi_{u,z}, \quad z = 0, \tag{2.1c}$$

$$\phi_{u,t} + g\eta_u = 0, \quad z = 0, \tag{2.1d}$$

$$\eta_{\ell,t} = \phi_{u,z}, \quad z = -h_u, \tag{2.1e}$$

$$\eta_{\ell,t} = \phi_{\ell,z}, \quad z = -h_u, \tag{2.1f}$$

$$\mathcal{R}(\phi_{u,t} + g\eta_\ell) = (\phi_{\ell,t} + g\eta_\ell), \quad z = -h_u, \tag{2.1g}$$

$$\phi_{\ell,z} = 0, \quad z = -h_u - h_\ell, \tag{2.1h}$$

where δ is the Dirac delta function, g the gravitational acceleration, and $x = x_0 + Ut$ the position of the moving source assumed to be in the upper fluid layer ($z_0 > -h_u$). The boundary-value problem for $\phi_{u/\ell}$, $\eta_{u/\ell}$ is complete with the imposition of an appropriate radiation condition, in this case a physical requirement that only waves with group velocity greater than (less than) the forward speed can be present far up (down) stream of the disturbance. If the source is located in the lower layer, the right-hand sides of (2.1) and (2.1b) are exchanged, but the remaining discussion in this section is unaffected.

Let us introduce the following normalizations:

$$t^* = \omega_0 t, \quad x^*, z^*, z_0^*, h^* = \frac{x, z, z_0, h_u}{H}, \quad \varphi_{u,\ell}^* = \frac{\phi_{u,\ell}}{\phi_0}, \quad m_0^* = \frac{m_0 H^2}{\phi_0}, \quad k^* = kH, \quad \omega^* = \frac{\omega}{\omega_0}, \tag{2.2}$$

where asterisks indicate dimensionless variables, $H = h_u + h_\ell$, and $\phi_0 = g\mathcal{A}/\omega_0$ scales the velocity potential where $\mathcal{A}$ is the characteristic wave amplitude. In a frame of reference moving with the source the dimensionless governing equations for velocity potentials, dropping all asterisks, are:

$$\nabla^2\varphi_u = m_0\delta(x - x_0, 0, z - z_0)\cos t, \quad -h < z < 0, \tag{2.3a}$$

$$\nabla^2\varphi_\ell = 0, \quad -1 < z < -h, \tag{2.3b}$$

$$\tau^2\varphi_{u,tt} - 2\tau\mathcal{F}\varphi_{u,xt} + \mathcal{F}^2\varphi_{u,xx} + \mathcal{F}\varphi_{u,z} = 0, \quad z = 0, \tag{2.3c}$$

$$\varphi_{u,z} = \varphi_{\ell,z}, \quad z = -h \tag{2.3d}$$

$$\mathcal{R}(\tau^2\varphi_{u,tt} - 2\tau\mathcal{F}\varphi_{u,xt} + \mathcal{F}^2\varphi_{u,xx} + \mathcal{F}\varphi_{u,z}) = \tau^2\varphi_{\ell,tt} - 2\tau\mathcal{F}\varphi_{\ell,xt} + \mathcal{F}^2\varphi_{\ell,xx} + \mathcal{F}\varphi_{\ell,z}, \quad z = -h, \tag{2.3e}$$

$$\varphi_{\ell,z} = 0, \quad z = -1, \tag{2.3f}$$

where $\tau = U\omega_0/g$ and $\mathcal{F} = U^2/gH$. Before deriving the solution to (2.3), some insights can be obtained from the dispersion relation. The solution for a free plane propagating wave, in a space-fixed coordinate system, in a two-layer fluid can be written as (see [18])

$$\eta_u = a\, \mathrm{e}^{\mathrm{i}(\mathbf{k}\cdot\mathbf{x} - \omega t)}, \tag{2.4a}$$

$$\eta_\ell = b\, \mathrm{e}^{\mathrm{i}(\mathbf{k}\cdot\mathbf{x} - \omega t)}, \tag{2.4b}$$

$$\varphi_u = -\mathrm{i}(A\cosh kz + B\sinh kz)\, \mathrm{e}^{\mathrm{i}(\mathbf{k}\cdot\mathbf{x} - \omega t)}, \tag{2.4c}$$

$$\varphi_\ell = -\mathrm{i}C\cosh k(z+1)\, \mathrm{e}^{\mathrm{i}(\mathbf{k}\cdot\mathbf{x} - \omega t)}, \tag{2.4d}$$

where $k = |\mathbf{k}|$. Coefficients a and b (both non-dimensionalized by $\mathcal{A}$) are amplitudes of surface and interfacial elevations, and are related by

$$\frac{b}{a} = \cosh kh - \frac{\alpha k}{\omega^2}\sinh kh. \tag{2.5}$$

where $\alpha \equiv \mathcal{F}/\tau^2$. In terms of a and b, the coefficients A, B and C are given by

$$A = \frac{a}{\omega}, \quad B = \frac{\omega a}{\alpha k}, \quad C = \frac{\omega b}{\alpha k \sinh k(1-h)}. \tag{2.6}$$

In (2.4a), the pair (k, ω) satisfy the dispersion relation:

$$\mathcal{D}(\omega, k) = \omega^4[\mathcal{R} + \coth kh\ \coth k(1-h)] - \alpha\omega^2 k[\coth kh + \coth k(1-h)] + \alpha^2k^2(1-\mathcal{R}) = 0. \tag{2.7}$$

It is easy to see that, for a given wavenumber $k > 0$, Eq. 2.7 has four solutions: $\pm\omega_s(k)$, $\pm\omega_i(k)$, with $\omega_s > \omega_i > 0$ [19], where $\pm\omega_s(k)$ and $\pm\omega_i(k)$ are denoted as the surface-mode and internal-mode waves, respectively [20].

In a frame of reference moving with the source, the only possible far-field free waves are those whose encounter frequencies are the same as the frequency of oscillation of the disturbance. The encounter frequency of a free wave

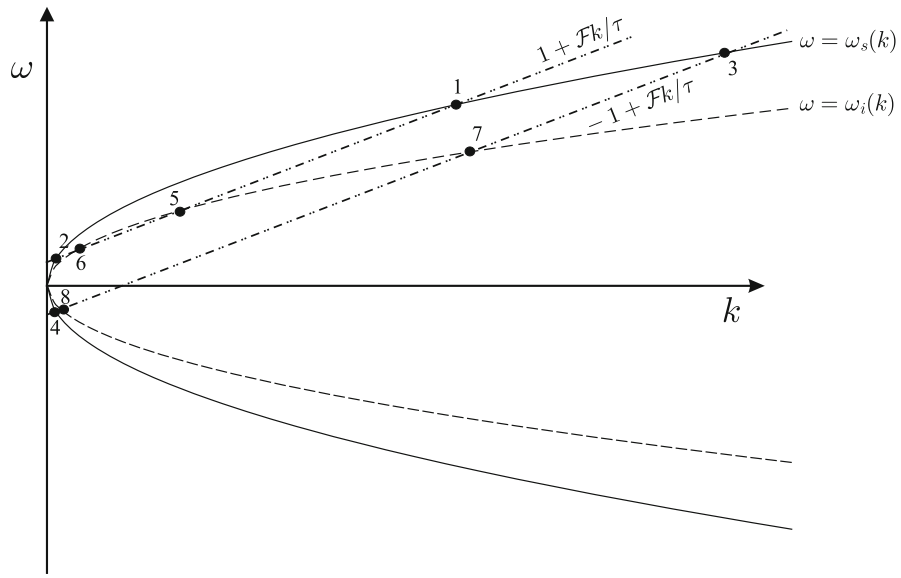

Fig. 1 Schematic of the dispersion relationship for far-field waves generated by a moving and oscillating disturbance in a two-layer density-stratified fluid. The figure also shows the numbering convention for these waves. Frequency lines $\omega = \pm 1 + \mathcal{F}k/\tau$: — · · —, can have up to $N_W = 8$ intersections with the internal (- - -) and surface (——) mode solutions of the dispersion relation (2.7)

is defined by $\omega_{\text{en}} = \omega \pm Uk$ where (k, ω) are the wavenumber and frequency of the free wave, U is speed of the source, and the positive/negative sign is taken if the source moves in the opposite/same direction as the free wave; see for example [21]. Therefore, the far-field waves of a translating/oscillating source correspond to the solutions to the dispersion relation (2.7) by letting ω=$\omega_0 \pm kU$ or equivalently:

$$\mathcal{D}(\pm 1 + \mathcal{F}k/\tau, k) = 0. \tag{2.8}$$

Roots of (2.8) are at the intersections of the surface and internal mode branches of stationary frame dispersion relation (2.7) (Fig. 1, solid and dashed curves, respectively) with the frequency lines, i.e., $\omega(k) = \pm 1 + \mathcal{F}k/\tau$ (Fig. 1, dash-dot lines). Figure 1 also defines the numbering convention for these roots where surface mode waves are denoted by wavenumbers k_1, k_2, k_3, k_4 (to be consistent with one-layer convention, (see e.g. [9]), and internal mode waves are denoted by wavenumbers k_5, k_6, k_7 and k_8.

When the encounter-frequency line becomes tangent to one of the dispersion relation branches, two of the roots coalesce, and the critical frequencies at which this occurs are labeled by $\tau_{\text{cr},s}$ or $\tau_{\text{cr},i}$ according to whether it is the $\omega_s(k)$ or $\omega_i(k)$ branch of the dispersion relation. Generally, we have for $\tau > \tau_{\text{cr},s}$, $N_W = 4$; for $\tau_{\text{cr},i} < \tau < \tau_{\text{cr},s}$, $N_W = 6$; and for $\tau < \tau_{\text{cr},i}$, $N_W = 8$ far-field waves associated with the oscillating and translating disturbance.

In general, waves associated with k_p, $p = 3, 4, 7, 8$, (the "p waves") are always present regardless of the physical parameters; however, those associated with k_q, $q = 1, 2, 5, 6$, (the "q" waves) may not exist depending on the value of τ_{cr}. Qualitatively, p/q waves have smaller/greater phase speed compared to U.

The dimensionless critical frequencies $\tau_{\text{cr},s}$, $\tau_{\text{cr},i}$ are functions of $\mathcal{R}$, $\mathcal{F}$ and h and can be found numerically. Figure 2 shows the dependence of $\tau_{\text{cr},s}$, $\tau_{\text{cr},i}$ on $\mathcal{F}$ and h for $\mathcal{R} = 0.2$ and 0.95. It is seen that $\tau_{\text{cr},s}$ has a weak dependence on h and $\mathcal{R}$ while $\tau_{\text{cr},i}$ has a relatively stronger dependence.

We note that no real surface/interface τ_{cr} can be found if

$$\mathcal{F} > \frac{1}{2}\left(1 \pm \sqrt{1 - 4h(1-h)(1-\mathcal{R})}\right) \equiv \mathcal{F}_{\text{cr}}, \tag{2.9}$$

where +/− refers to the surface/internal mode. Figure 3 shows the variation of $\mathcal{F}_{\text{cr}}$ with $\mathcal{R}$ and h. For $\mathcal{R}$ close to unity, the critical Froude number associated with the surface mode, $\mathcal{F}_{\text{cr},s} \approx 1$, and that associated with the internal mode, $\mathcal{F}_{\text{cr},s} \approx 0$. Thus in a realistic ocean where $1 - \mathcal{R}$ is small, no internal wave propagates ahead of

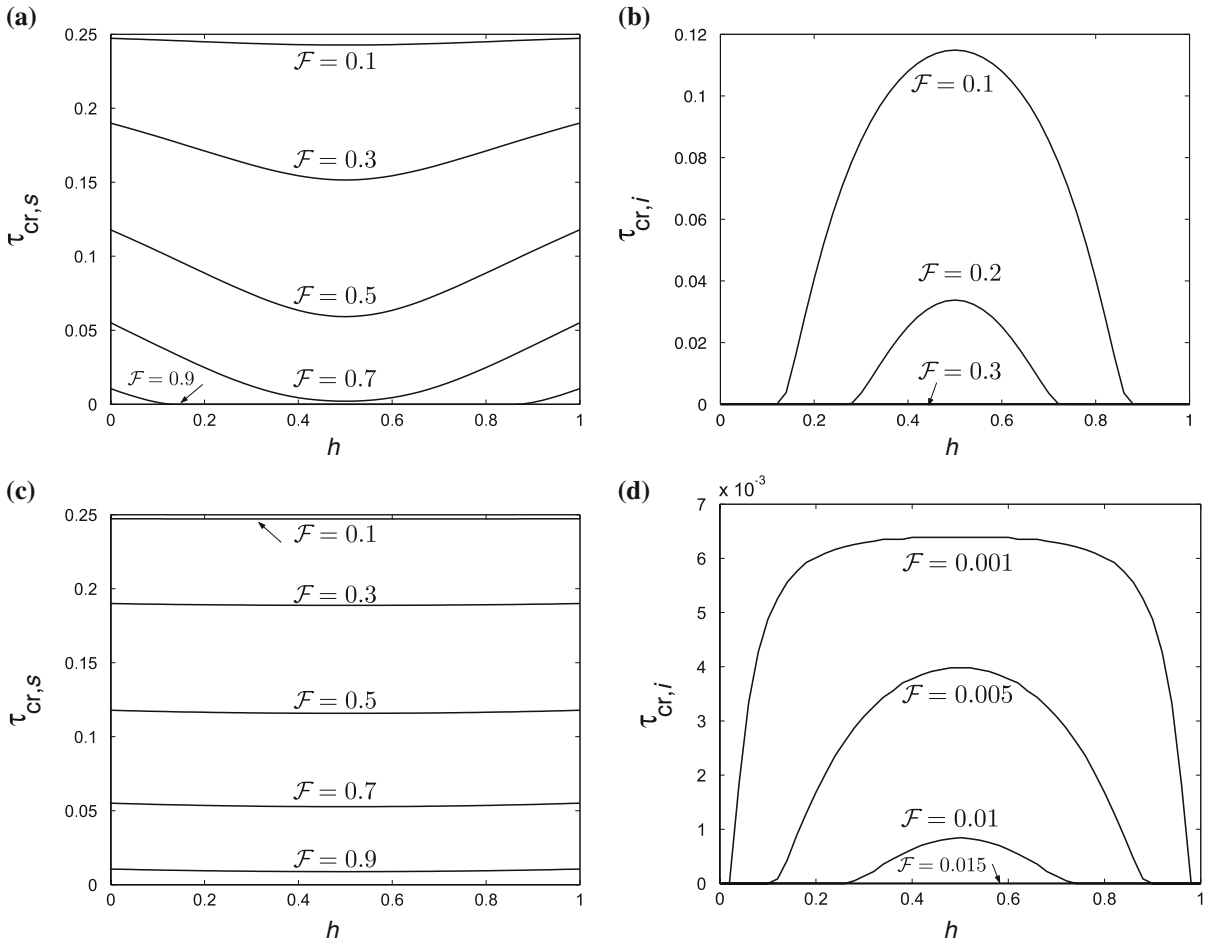

Fig. 2 Critical dimensionless frequencies $\tau_{\mathrm{cr},s}$, $\tau_{\mathrm{cr},i}$ as a functions of depth ratio h for different Froude numbers $\mathcal{F}$

the disturbance unless $\mathcal{F}$ is comparably small. For given $\mathcal{R}$, the maximum range of $\mathcal{F}$ for upstream waves occurs at $h = 0.5$ where $\mathcal{F}_{\mathrm{cr}}$ are extremal. It is noted that in the limit of $1 - \mathcal{R} \to 0$ all classical results for waves of an oscillating/translating source in a homogeneous fluid (e.g. [4]) are retrieved.

In the limiting case of deep layers, $kh, k(1-h) \gg 1$, the far-field wavenumbers in two dimensions can be obtained in a closed form. In this limit, (2.7) reduces to:

$$\omega_s^2 = \alpha k, \quad \omega_i^2 = \alpha k \vartheta \tag{2.10}$$

where $\vartheta = (1-\mathcal{R})/(1+\mathcal{R})$. The resultant waves at infinity are solutions of the following eight equations

$$\pm 1 + \mathcal{F}k/\tau = \pm\sqrt{\alpha k}, \quad \pm 1 + \mathcal{F}k/\tau = \pm\sqrt{\alpha k \vartheta}\ . \tag{2.11}$$

Depending on the values of τ and $\mathcal{R}$, and the sign before unity, each of these eight equations can have either two or zero real roots. The first equation of (2.11) is for surface-mode waves and is the same as that for homogeneous fluid. The second equation of (2.11) is for internal-mode waves where the effect of gravitational acceleration is effectively reduced by the factor of ϑ. The roots to (2.11) are:

$$k_{1,2} = \frac{1}{2\alpha\tau^2}\left[1 - 2\tau \pm (1-4\tau)^{\frac{1}{2}}\right], \tag{2.12}$$

$$k_{3,4} = \frac{1}{2\alpha\tau^2}\left[1 + 2\tau \pm (1+4\tau)^{\frac{1}{2}}\right], \tag{2.13}$$

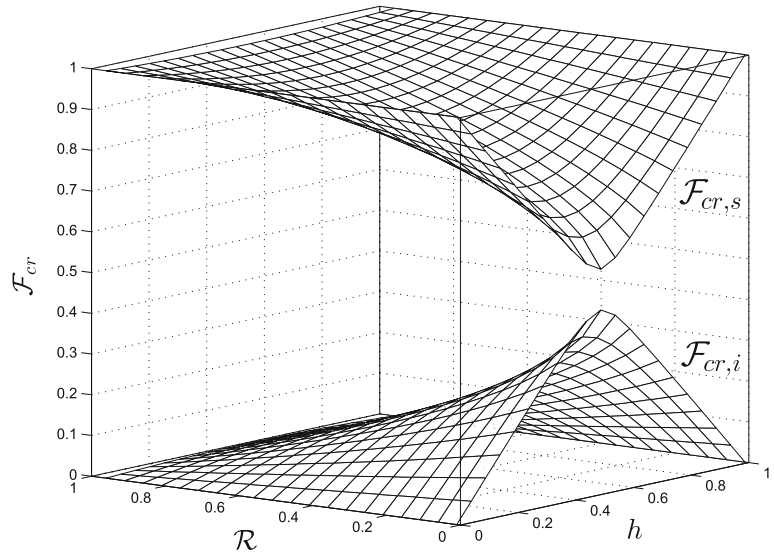

Fig. 3 Critical Froude numbers $\mathcal{F}_{\mathrm{cr},s}$, $\mathcal{F}_{\mathrm{cr},i}$ as functions of $\mathcal{R}$ and h

$$k_{5,6} = \frac{1}{2\alpha\vartheta\tau_\ell^2}\left[1 - 2\tau_\ell \pm (1-4\tau_\ell)^{\frac{1}{2}}\right], \tag{2.14}$$

$$k_{7,8} = \frac{1}{2\alpha\vartheta\tau_\ell^2}\left[1 + 2\tau_\ell \pm (1+4\tau_\ell)^{\frac{1}{2}}\right], \tag{2.15}$$

where $\tau_\ell = \tau/\vartheta$. It is clear that: $N_W = 4$ for $\tau > 1/4$; $N_W = 6$ for $0.25\vartheta < \tau < 1/4$; and $N_W = 8$ for $\tau < 0.25\vartheta$.

In a stationary frame, the surface/internal wave associated with k_4/k_8 propagates backward (negative phase and group speed C_p, $C_g < 0$); the other waves propagate forward (C_p, $C_g > 0$) with the k_2/k_6 waves, if they exist, moving ahead of the disturbance ($C_g > U$), and the k_1/k_5 and k_3/k_7 waves trailing behind the disturbance ($C_g < U$). The difference between the two latter pairs of waves is that $C_p > U$ for k_1/k_5, if they exist, and $C_p < U$ for k_3, k_7.

3 Green function

The kinematic analysis of the preceding section gives wavenumbers of the waves that appear at the far field of an oscillating translating disturbance in a two-layer density-stratified fluid. To determine the amplitudes of these waves and also surface and interface elevations in the near field of the disturbance, the boundary-value problem needs to be solved analytically. In this section, we obtain the Green function in two dimensions for the velocity potential associated with a steadily translating point source of sinusoidally oscillating strength in a two-layer density-stratified fluid. For the source located in the upper layer we present the general form of the two-dimensional Green function, and study the limiting case of deep layers where the expressions are simplified considerably. The corresponding Green function for the source in the lower layer is given in Sect. 3.3. Extension of the these results to three dimensions is straightforward and the final results are given in the Appendix.

3.1 Two-dimensional source in the upper layer

We seek a steady solution to the governing equation (2.3) in the frame of reference moving with the source. Let us assume:

$$\varphi_u(x,z,t) = \mathfrak{Re}\{m_0\,\phi_u(x,z)\,\mathrm{e}^{\mathrm{i}t}\}, \quad \varphi_\ell(x,z,t) = \mathfrak{Re}\{m_0\,\phi_\ell(x,z)\,\mathrm{e}^{\mathrm{i}t}\}, \tag{3.16}$$

and consider a solution of the following form:

$$\phi_u = \frac{\log r}{2\pi} + \frac{\log r_2}{2\pi} + \mathcal{H}_u(x,z), \phi_\ell = \mathcal{H}_\ell(x,z), \tag{3.17}$$

where

$$r^2 = x^2 + (z - z_0)^2, \quad r_2^2 = x^2 + (z + z_0 + 2h)^2. \tag{3.18}$$

To solve for $\mathcal{H}_u$, $\mathcal{H}_\ell$, we apply a Fourier transform in x (see [5]). The function $\log(r)$ in two dimensions does not have a Fourier transform (see [22] for a variant definition using Laplace equation), however, we can write it in an integral form:

$$\log\sqrt{x^2 + a^2} = -\int_0^\infty \frac{\mathrm{e}^{-ka}\cos kx - \cos k}{k}\mathrm{d}k. \tag{3.19}$$

The second term in the numerator is not a function of x, z. However, it enters the boundary-value problem through $\varphi_{u/\ell,tt}$ (Eq. 2.3c, e). In [23] the potential of the virtual singularity is subtracted from the real singularity (i.e., $\log r - \log r_2$) to avoid the new term under the integral. Debnath [24] used an expression similar to ours without the constant term (see the definition of M_1 after Eq. 34 in his paper and compare with his Eq. 22) which strictly does not admit an inverse Fourier transform.

The integral form of the logarithmic function being available, the solution to the boundary-value problem (2.3) can be written in terms of inverse Fourier integrals:

$$\begin{aligned}\phi_u = \frac{\log r}{2\pi} + \frac{\log r_2}{2\pi} + \int_0^\infty \Big[&(A^+\cosh kz + B^+\sinh kz)\,\frac{\mathrm{e}^{\mathrm{i}kx}}{2} \\ &+(A^-\cosh kz + B^-\sinh kz)\,\frac{\mathrm{e}^{-\mathrm{i}kx}}{2} - \frac{\cos k}{\pi k}\Big]\,\mathrm{d}k,\end{aligned} \tag{3.20}$$

$$\phi_\ell = \int_0^\infty \left[C^+\cosh k(z+1)\,\frac{\mathrm{e}^{\mathrm{i}kx}}{2} + C^-\cosh k(z+1)\,\frac{\mathrm{e}^{-\mathrm{i}kx}}{2}\right]\mathrm{d}k. \tag{3.21}$$

Upon substitution of the boundary conditions, the coefficients $A^\pm$, $B^\pm$ and $C^\pm$ can be found:

$$X^\pm = \frac{\alpha\hat{X}^\pm}{\lambda^{\pm 4} - (\omega_s^2 + \omega_i^2)\lambda^{\pm 2} + \omega_s^2\omega_i^2}, \tag{3.22}$$

where X can be either of A, B or C with

$$\hat{A}^\pm = \beta\,\lambda^{\pm 4} + \frac{\alpha k\,(-\mathcal{R}\mathrm{sl}\,\gamma + \mathrm{cl}\,\mathrm{cu}\,\beta + \mathcal{R}\mathrm{sl}\,\mathrm{su}\,\beta - \mathrm{sl}\,\beta\,\mathrm{cu} + \mathrm{sl}\,\mathcal{R}\beta\,\mathrm{cu})\,\lambda^{\pm 2}}{\mathrm{sl}\,\mathrm{su}\,\mathcal{R} + \mathrm{cu}\,\mathrm{cl}} + \frac{\alpha^2k^2\mathrm{sl}\,\mathrm{cu}\,\beta\,(-1+\mathcal{R})}{\mathrm{sl}\,\mathrm{su}\,\mathcal{R} + \mathrm{cu}\,\mathrm{cl}}, \tag{3.23}$$

$$\begin{aligned}\hat{B}^\pm = &\frac{(\mathrm{sl}\,\mathrm{cu}\,\mathcal{R}\beta + \beta\,\mathrm{cl}\,\mathrm{su} - \mathcal{R}\mathrm{sl}\,\gamma)\,\lambda^{\pm 4}}{\mathrm{sl}\,\mathrm{su}\,\mathcal{R} + \mathrm{cu}\,\mathrm{cl}} + \frac{\alpha k\beta\,(\mathrm{sl}\,\mathrm{cu}\,\mathcal{R} + \mathrm{cl}\,\mathrm{su} - \mathrm{sl}\,\mathrm{su} + \mathrm{sl}\,\mathrm{su}\,\mathcal{R})\,\lambda^{\pm 2}}{\mathrm{sl}\,\mathrm{su}\,\mathcal{R} + \mathrm{cu}\,\mathrm{cl}} \\ &+\frac{\alpha^2k^2\beta\,\mathrm{sl}\,\mathrm{su}\,(-1+\mathcal{R})}{\mathrm{sl}\,\mathrm{su}\,\mathcal{R} + \mathrm{cu}\,\mathrm{cl}},\end{aligned} \tag{3.24}$$

$$\hat{C}^\pm = \frac{\mathcal{R}\left(\mathrm{cu}^2\beta - \mathrm{cu}\,\gamma - \mathrm{su}^2\beta\right)\lambda^{\pm 4}}{\mathrm{cu}\,\mathrm{cl} + \mathrm{sl}\,\mathrm{su}\,\mathcal{R}} + \frac{\mathcal{R}\alpha k\left(-\mathrm{su}^2\beta + \mathrm{cu}^2\beta + \mathrm{su}\,\gamma\right)\lambda^{\pm 2}}{\mathrm{cu}\,\mathrm{cl} + \mathrm{sl}\,\mathrm{su}\,\mathcal{R}}, \tag{3.25}$$

where

$$\begin{aligned}&\lambda^\pm = 1 \mp \mathcal{F}k/\tau, \quad \beta = \frac{\cosh k(z_0+h)}{\pi\ \alpha k\ \exp(kh)}, \quad \gamma = \frac{\mathrm{e}^{-k(z_0+h)}}{\pi\alpha k} \\ &\mathrm{su} \equiv \sinh(kh), \quad \mathrm{cu} \equiv \cosh(kh), \\ &\mathrm{sl} \equiv \sinh[k(1-h)], \quad \mathrm{cl} \equiv \cosh[k(1-h)],\end{aligned} \tag{3.26}$$

and the $\omega_{s,i}$ are surface-mode and internal-mode solutions to the dispersion relation (2.7) for a given k.

From (2.1c) and (2.1e), the surface and interface elevations are obtained:

$$\eta_u = \varphi_{u,t} - \frac{\mathcal{F}}{\tau}\varphi_{u,x}, \quad z = 0, \tag{3.27}$$

$$\eta_\ell = \frac{\mathcal{R}(\varphi_{u,t} - \mathcal{F}/\tau\ \varphi_{u,x}) - (\varphi_{\ell,t} - \mathcal{F}/\tau\ \varphi_{\ell,x})}{(1-\mathcal{R})}, \quad z = -h. \tag{3.28}$$

For numerical evaluation of (3.20) and (3.21), the integrals can be transformed into Cauchy principal-value integrals. To do this, one may finally express (3.20) and (3.21) in the expanded form:

$$\phi_u = \frac{\log r}{2\pi} + \frac{\log r_2}{2\pi} + \int_0^\infty \left[\frac{(\hat{A}^+ \cosh kz + \hat{B}^+ \sinh kz)}{2\,\mathcal{G}^+}\, \mathrm{e}^{\mathrm{i}kx} + \frac{(\hat{A}^- \cosh kz + \hat{B}^- \sinh kz)}{2\,\mathcal{G}^-}\, \mathrm{e}^{-\mathrm{i}kx} - \frac{\cos k}{\pi k} \right] \mathrm{d}k, \tag{3.29}$$

$$\phi_\ell = \int_0^\infty \left[\frac{\hat{C}^+}{2\,\mathcal{G}^+} \cosh k(z+1)\, \mathrm{e}^{\mathrm{i}kx} + \frac{\hat{C}^-}{2\,\mathcal{G}^-} \cosh k(z+1)\, \mathrm{e}^{-\mathrm{i}kx} \right] \mathrm{d}k, \tag{3.30}$$

where

$$\mathcal{G}^\pm/\alpha = \lambda^{\pm 4} - (\omega_s^2 + \omega_i^2)\lambda^{\pm 2} + \omega_s^2\omega_i^2\ . \tag{3.31}$$

Here $\mathcal{G}^+$ can have a maximum number of four real roots while $\mathcal{G}^-$ always has four real roots. Assuming all eight real roots exist, one may finally express (3.20) and (3.21) as:

$$\begin{aligned}\phi_u = {} & \frac{\log r}{2\pi} + \frac{\log r_2}{2\pi} + \sum_{k=k_1,k_2,k_5,k_6} (-1)^w \mathrm{i}\pi \frac{(\hat{A}^+ \cosh kz + \hat{B}^+ \sinh kz)}{2\,\mathcal{I}^+}\, \mathrm{e}^{\mathrm{i}kx} \\ & + \sum_{k=k_3,k_4,k_7,k_8} (-1)^w \mathrm{i}\pi \frac{(\hat{A}^- \cosh kz + \hat{B}^- \sinh kz)}{2\,\mathcal{I}^-}\, \mathrm{e}^{-\mathrm{i}kx} \\ & + \mathrm{PV} \int_0^\infty \left[\frac{(\hat{A}^+ \cosh kz + \hat{B}^+ \sinh kz)}{2\,\mathcal{G}^+}\, \mathrm{e}^{\mathrm{i}kx} + \frac{(\hat{A}^- \cosh kz + \hat{B}^- \sinh kz)}{2\,\mathcal{G}^-}\, \mathrm{e}^{-\mathrm{i}kx} - \frac{\cos k}{\pi k} \right] \mathrm{d}k, \end{aligned} \tag{3.32}$$

$$\begin{aligned}\phi_\ell = {} & \sum_{k=k_1,k_2,k_5,k_6} (-1)^w \mathrm{i}\pi \frac{\hat{C}^+}{2\,\mathcal{I}^+} \cosh k(z+1)\, \mathrm{e}^{\mathrm{i}kx} + \sum_{k=k_3,k_4,k_7,k_8} (-1)^w \mathrm{i}\pi \frac{\hat{C}^-}{2\,\mathcal{I}^-} \cosh k(z+1)\, \mathrm{e}^{-\mathrm{i}kx} \\ & + \mathrm{PV} \int_0^\infty \left[\frac{\hat{C}^+}{2\,\mathcal{G}^+} \cosh k(z+1)\, \mathrm{e}^{\mathrm{i}kx} + \frac{\hat{C}^-}{2\,\mathcal{G}^-} \cosh k(z+1)\, \mathrm{e}^{-\mathrm{i}kx} \right] \mathrm{d}k, \end{aligned} \tag{3.33}$$

where

$$\mathcal{I}^\pm/\alpha = \frac{\mathrm{d}}{\mathrm{d}k} \left\{ \lambda^{\pm 4} - (\omega_s^2 + \omega_i^2)\lambda^{\pm 2} + \omega_s^2\omega_i^2 \right\} \tag{3.34}$$

and $w = 1$ for $k = k_2, k_6$, and $w = 2$ otherwise. If any of k_1, k_2, k_5, k_6 is not real (they disappear as "pairs"), the corresponding term in the sum is skipped.

The far-field amplitudes can be found by contour integration of (3.20) and (3.21). About each singularity, however, there exist two choices of indentation of the path with each leading to a different solution. Careful consideration of these possibilities for each singularity shows that one of them is associated with a wave coming from infinity, which is in contradiction with the radiation condition (scattering energy of a source must flow toward infinity). Thus, this solution should not be chosen. Note that waves of a moving source can propagate both fore and aft of the disturbance as long as they move away from the source. This can be better understood by visualizing an oscillating but not translating source which sends out similar waves in both directions. Now, if the source moves slower than these waves, it will always stay behind fore waves.

In this problem, it is found that to satisfy the radiation condition of outgoing waves at infinity, the contour integration along the real k-axis must be indented below the poles for k_2, k_6 (if they exist) and above those associated with all the other wavenumbers. After some algebra, the final expressions for the far-field amplitudes are:

$$\phi_u^\infty = \pi \frac{\hat{A}^+ \cosh kz + \hat{B}^+ \sinh kz}{2\mathcal{I}^+}, \quad \phi_\ell^\infty = \pi \frac{\hat{C}^+ \cosh k(z+1)}{2\mathcal{I}^+}, \tag{3.35}$$

for $k = k_1, k_2, k_5, k_6$, and,

$$\phi_u^\infty = \pi \frac{\hat{A}^- \cosh kz + \hat{B}^- \sinh kz}{2\mathcal{I}^-}, \quad \phi_\ell^\infty = \pi \frac{\hat{C}^- \cosh k(z+1)}{2\mathcal{I}^-}, \tag{3.36}$$

for $k = k_3, k_4, k_7, k_8$.

Equivalently, as an alternative approach and to avoid encountering principal-value integrations, one can introduce a fictitious dissipation term to the governing equation (2.3) [18]. By the means of this damping term, the path integral will be off the x-axis and does not encounter any singularity. By setting this fictitious damping equal to zero, the potential solution is obtained ([15], for example). In fact it can be shown that the solution for a general accelerating/variable-strength source in a two-layer fluid (not presented here) in the limit of long time, steady motion and no oscillation asymptotically tends to the solution of [15].

3.2 Deep-layers limiting case

When both layers are deep, the Green function can be reduced to independent integrals in Fourier space. These reduced expressions are two-layer counterparts of the well known deep-water homogeneous-fluid Green function (see [8] for example).

The Green-function expressions depend on the value of τ relative to $\tau_{\mathrm{cr},i}$, $\tau_{\mathrm{cr},s}$. For $\tau < \tau_{\mathrm{cr},i}$, $N_W = 8$ distinct waves exist. After some algebra, the final form of the solution can be expressed as:

$$\begin{aligned}\phi_u = \frac{1}{2\pi}\log r + \frac{1}{2\pi}\log r_2 + \int_0^\infty \Bigg[& \frac{\hat{A}^+ \cosh kz + \hat{B}^+ \sinh kz}{2\,\tau^4} \sum_{q=1,2,5,6} \frac{a_q}{k-k_q}\, \mathrm{e}^{\mathrm{i}kx} \\ & + \frac{\hat{A}^- \cosh kz + \hat{B}^- \sinh kz}{2\,\tau^4} \sum_{q=3,4,7,8} \frac{a_q}{k-k_q}\, \mathrm{e}^{-\mathrm{i}kx} - \frac{\cos k}{\pi k} \Bigg]\, \mathrm{d}k, \end{aligned} \tag{3.37}$$

$$\phi_\ell = \int_0^\infty \left[\frac{\hat{C}^+\, \mathrm{e}^{\mathrm{i}kx}}{2\tau^4} \sum_{q=1,2,5,6} \frac{a_q}{k-k_q} + \frac{\hat{C}^-\, \mathrm{e}^{-\mathrm{i}kx}}{2\tau^4} \sum_{q=3,4,7,8} \frac{a_q}{k-k_q} \right] \cosh k(z+1)\, \mathrm{d}k, \tag{3.38}$$

where

$$a_q = \prod_{j=\{1,2,5,6\}-q} \frac{1}{\alpha^3} \cdot \frac{1}{k_q - k_j} \quad \text{for } q = 1, 2, 5, 6; \tag{3.39}$$

$$a_q = \prod_{j=\{3,4,7,8\}-q} \frac{1}{\alpha^3} \cdot \frac{1}{k_q - k_j} \quad \text{for } q = 3, 4, 7, 8. \tag{3.40}$$

The integrals contain simple poles at $k = k_1, \ldots, k_8$. It can be shown that the only valid (i.e., consistent with radiation condition) solution of this integral is obtained when the integration contour is indented below k_2, k_6 and above the singularities corresponding to the other wavenumbers.

For $\tau_{\mathrm{cr},i} < \tau < \tau_{\mathrm{cr},s}$, $N_W = 6$, and we have

$$\phi_u = \frac{1}{2\pi}\log r + \frac{1}{2\pi}\log r_2 + \int_0^\infty \left[\frac{\hat{A}^+ \cosh kz + \hat{B}^+ \sinh kz}{2\,\tau^4} \sum_{q=1,2} \frac{a_q}{k-k_q}\, \mathrm{e}^{\mathrm{i}kx} \right.$$
$$\left. + \frac{\hat{A}^- \cosh kz + \hat{B}^- \sinh kz}{2\,\tau^4} \sum_{q=3,4,7,8} \frac{a_q}{k-k_q}\, \mathrm{e}^{-\mathrm{i}kx} - \frac{\cos k}{\pi k} \right] \mathrm{d}k, \tag{3.41}$$

$$\phi_\ell = \int_0^\infty \left[\frac{\hat{C}^+ \,\mathrm{e}^{\mathrm{i}kx}}{2\tau^4} \sum_{q=1,2} \frac{a_q}{k-k_q} + \frac{\hat{C}^- \,\mathrm{e}^{-\mathrm{i}kx}}{2\tau^4} \sum_{q=3,4,7,8} \frac{a_q}{k-k_q} \right] \cosh k(z+1)\,\mathrm{d}k, \tag{3.42}$$

where now

$$a_1 = \frac{1}{\alpha} \cdot \frac{\tau^2}{\lambda^2(k_1) - \omega_i^2(k_1)} \cdot \frac{1}{k_1 - k_2}, \tag{3.43}$$

$$a_2 = \frac{1}{\alpha} \cdot \frac{\tau^2}{\lambda^2(k_2) - \omega_i^2(k_2)} \cdot \frac{1}{k_2 - k_1} \tag{3.44}$$

and

$$a_q = \prod_{j=\{3,4,7,8\}-q} \frac{1}{\alpha^3} \cdot \frac{1}{k_q - k_j} \quad \text{for } q = 3, 4, 7, 8 \tag{3.45}$$

and the contour integrations for (3.41) and (3.42) (and below) must be treated similarly to satisfy the radiation condition.

Finally, for $\tau > \tau_{\mathrm{cr},s}$, $N_W = 4$, and we have

$$\phi_u = \frac{1}{2\pi}\log r + \frac{1}{2\pi}\log r_2 + \int_0^\infty \left\{ \frac{\hat{A}^- \cosh kz + \hat{B}^- \sinh kz}{2\,\tau^4} \sum_{q=3,4,7,8} \frac{a_q}{k-k_q}\, \mathrm{e}^{-\mathrm{i}kx} - \frac{\cos k}{\pi k} \right\} \mathrm{d}k, \tag{3.46}$$

$$\phi_\ell = \int_0^\infty \frac{\hat{C}^- \,\mathrm{e}^{-\mathrm{i}kx}}{2\tau^4} \sum_{q=3,4,7,8} \frac{a_q}{k-k_q} \cosh k(z+1)\,\mathrm{d}k, \tag{3.47}$$

where

$$a_q = \prod_{j=\{3,4,7,8\}-q} \frac{1}{\alpha^3} \cdot \frac{1}{k_q - k_j} \quad \text{for } q = 3, 4, 7, 8. \tag{3.48}$$

3.3 Source in the lower layer

For the source point in the lower layer, the derivation is quite similar and the details are omitted. Here we provide the final expressions for the Green functions:

$$\phi_u = \int_0^\infty \left[(A^+ \cosh kz + B^+ \sinh kz)\, \frac{\mathrm{e}^{\mathrm{i}kx}}{2} + (A^- \cosh kz + B^- \sinh kz)\, \frac{\mathrm{e}^{-\mathrm{i}kx}}{2} \right] \mathrm{d}k, \tag{3.49}$$

$$\phi_\ell = \frac{\log r}{2\pi} + \frac{\log r_3}{2\pi} + \int_0^\infty \left[C^+ \cosh k(z+1)\, \frac{\mathrm{e}^{\mathrm{i}kx}}{2} + C^- \cosh k(z+1)\, \frac{\mathrm{e}^{-\mathrm{i}kx}}{2} - \frac{\cos k}{\pi k} \right] \mathrm{d}k, \tag{3.50}$$

where $r_3^2 \equiv x^2 + (2+z+z_0)^2$. By applying the boundary conditions, the coefficients $A^\pm$, $B^\pm$ and $C^\pm$ are obtained:

$$X^\pm = \frac{\alpha \hat{X}^\pm}{\lambda^{\pm 4} - (\omega_s^2 + \omega_i^2)\lambda^{\pm 2} + \omega_s^2 \omega_i^2}, \tag{3.51}$$

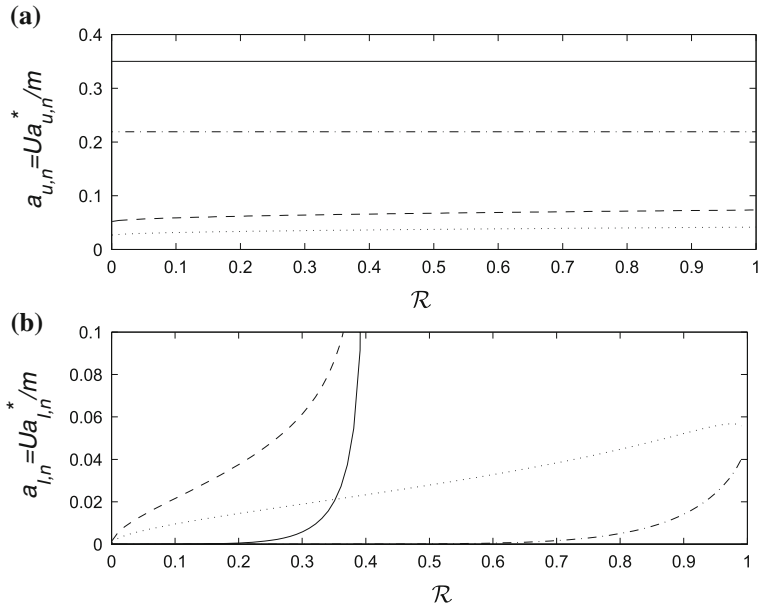

Fig. 4 Far-field wave amplitudes $a_{u,n}$, $a_{\ell,n}$, as functions of $\mathcal{R}$ for $\mathcal{F}=0.03$, $\tau=0.1$, $z_0=-0.02$, $h=0.5$. **a** For $a_{u,n}$: $a_{u,1}$ ——; $a_{u,2}$ - - -; $a_{u,3}$ – · –; and $a_{u,4}$ · · ·. **b** for $a_{\ell,n}$: $a_{\ell,5}$ ——; $a_{\ell,6}$ - - -; $a_{\ell,7}$ – · –; and $a_{\ell,8}$ · · ·

where X is either of A, B or C and

$$\hat{A}^{\pm}=\frac{\alpha k\lambda^{\pm^2}\beta\ (\mathrm{sl}+\mathrm{cl})}{\mathrm{sl}\,\mathcal{R}\mathrm{su}+\mathrm{cl}\,\mathrm{cu}},\quad \hat{B}^{\pm}=\frac{\lambda^{\pm^4}\beta\ (\mathrm{sl}+\mathrm{cl})}{\mathrm{sl}\,\mathrm{su}\,\mathcal{R}+\mathrm{cl}\,\mathrm{cu}}, \tag{3.52}$$

$$\hat{C}^{\pm}=-\frac{\beta\ (\mathrm{su}\,\mathcal{R}-\mathrm{cu})\,\lambda^{\pm^4}}{\mathrm{sl}\,\mathrm{su}\,\mathcal{R}+\mathrm{cl}\,\mathrm{cu}}+\frac{\beta\,\alpha k\,(-\mathrm{su}+\mathrm{cu})\,\lambda^{\pm^2}}{\mathrm{sl}\,\mathrm{su}\,\mathcal{R}+\mathrm{cl}\,\mathrm{cu}}+\frac{\beta\,\alpha^2k^2\mathrm{su}\ (\mathcal{R}-1)}{\mathrm{sl}\,\mathrm{su}\,\mathcal{R}+\mathrm{cl}\,\mathrm{cu}}, \tag{3.53}$$

where now

$$\beta=\frac{\cosh k(z_0+1)}{\pi\ \alpha\ k\ \mathrm{e}^{k(1-h)}}. \tag{3.54}$$

3.4 Discussion

The Green functions we obtained provide the solution everywhere in the flow. Of special interest are the wave amplitudes in the far field. These wave amplitudes, in general $a_{u,n}$, $a_{\ell,n}$, $n=1,\ldots,8$, on the upper (surface), lower (interfacial) layers, depend on the characteristics of the moving oscillating source, τ, $\mathcal{F}$ and z_0, as well as those of the ocean environment, h and $\mathcal{R}$.

Figures 4a and b plot $a_{u,n}$, $n=1$, 2, 3, 4, and $a_{\ell,n}$, $n=5$, 6, 7, 8, respectively, for the surface and internal mode waves as a function of the density ratio $\mathcal{R}$. The other parameters used are $\mathcal{F}=0.032$, $\tau=0.1$, $h=0.5$, and $z_0=-0.02$. With the source in the upper layer in this case, the dependence on $\mathcal{R}$ of $a_{u,n}$ is relatively weak, while $a_{\ell,n}$ generally increase with $\mathcal{R}$ (with a rate that depends on the specific mode n). This is expected because, relative to the density of the lower fluid, the momentum introduced by the source in the upper layer increases as $\mathcal{R}$ increases. For other parameters fixed, $\tau_{\mathrm{cr},i}$ decreases as $\mathcal{R}$ increases. Beyond a certain value of $\mathcal{R}$ ($\mathcal{R}=0.4$ in this case), $\tau_{\mathrm{cr},i}<\tau$, N_W decreases from 8 to 6, and the amplitudes associated with the two modes that are eliminated blow up (corresponding to their group velocity approaching to U). Based on Fig. 4, hereafter, we focus on two values of density ratio, $\mathcal{R}=0.2$ and 0.95; only the latter value, of course, corresponds to conditions in the physical ocean.

Figures 5a–d show the dependence of a_n on $\mathcal{F}$ for $\mathcal{R}=0.2$, 0.95. With $\mathcal{F}$ varying, a_n are now non-dimensionalized by $g/(m\omega_0)$. Other physical parameters are $\tau=0.1$, $h=0.5$, and $z_0=-0.02$. Generally, as $\mathcal{F}$ increases, there

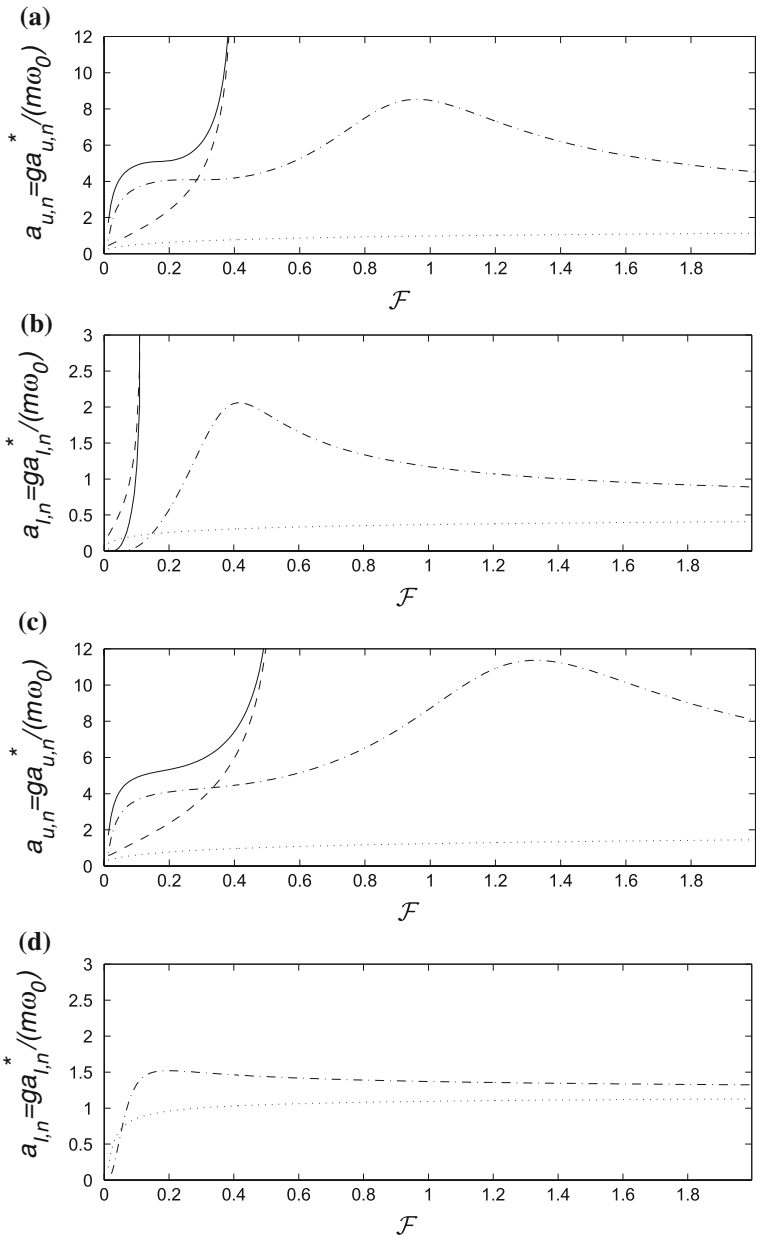

Fig. 5 Far-field wave amplitudes $a_{u,n}$, $a_{\ell,n}$, as functions of $\mathcal{F}$ for $\tau = 0.1$, $z_0 = -0.02$, $h = 0.5$, and, **a, b** $\mathcal{R} = 0.2$; **c, d** $\mathcal{R} = 0.95$. In Figs. 5 **a, c** for $a_{u,n}$: $a_{u,1}$ ——— ; $a_{u,2}$ - - - ; $a_{u,3}$ – · – ; and $a_{u,4}$ · · · . In Figs. 5 **b, d** for $a_{\ell,n}$: $a_{\ell,5}$ ——— ; $a_{\ell,6}$ - - - ; $a_{\ell,7}$ – · – ; and $a_{\ell,8}$ · · ·

are values $\mathcal{F} = \mathcal{F}_{\max}$, at which $a_{u,3}$ and $a_{\ell,7}$ obtain maximum and then decay. If the range of $\mathcal{F}$ in Fig. 5 is extended, we find that this is in fact the case for all p waves. Similar to previous figures, there are critical values $\mathcal{F}_{\rm cr}$, given the other parameters, beyond which respective q waves disappear; with the general feature that the corresponding amplitudes become unbounded as $\mathcal{F}$ approached these $\mathcal{F}_{\rm cr}$ values. The magnitude of $\mathcal{R}$ affects the values of $\mathcal{F}_{\max}$ and $\mathcal{F}_{\rm cr}$, with these values greater/smaller for the surface/internal mode wave amplitudes for larger $\mathcal{R}$.

Dependence of a_n on τ and h is more uniform. For a source near the free surface as τ increases the amplitudes of the p/q waves decrease/increase. If τ approaches $\tau_{{\rm cr},s}$, $\tau_{{\rm cr},i}$, the respective q wave amplitudes become unbounded and disappear. In the limit $\tau \to 0$, i.e., a steady translating source, the wavenumbers associated

with, respectively, $a_{u,1}$, $a_{u,3}$ and $a_{\ell,5}$, $a_{\ell,7}$ coincide and their amplitudes become equal. In this limit, the wavenumbers associated with $a_{u,2}$, $a_{u,4}$ and $a_{\ell,6}$, $a_{\ell,8}$ go to zero but the amplitudes remain finite. As z_0 decreases towards the interface, $a_{\ell,n}$ does not change appreciably, while $a_{u,n}$ decreases significantly. The main difference between $\mathcal{R} = 0.2$ and $\mathcal{R} = 0.95$ is that, for the latter, $\tau_{\mathrm{cr},i} = 0$ and the $a_{\ell,5}$ and $a_{\ell,6}$ waves do not exist ($N_W = 6$). In fact, for $\mathcal{F} < 0.5$, it can be shown from (2.9) that the maximum $\mathcal{R}$ for $a_{\ell,5}$ and $a_{\ell,6}$ waves to exist is given by:

$$\mathcal{R}_{\max} = 1 - \frac{\mathcal{F}}{h(1-h)}(1-\mathcal{F}). \tag{3.55}$$

A similar expression can be obtained for $\mathcal{F} > 0.5$.

In the ocean, h (for given total depth H) can vary significantly due to the passage of long interfacial waves. In littoral zones, the amplitude of these waves can be an appreciable fraction of H (see e.g. [25]). Again, if the source is located near the free surface, then most of the variations in the far-field wave amplitudes occur for smaller h. As h increases, $a_{u,n}/a_{\ell,n}$ generally increases/diminishes. These dependencies are more prominent for $a_{\ell,n}$. In particular, for small enough $\mathcal{R}$, there is a critical depth ratio near which $a_{\ell,5}$ and $a_{\ell,6}$ go unbounded and below which they disappear. For a more physically relevant case of weak stratification ($1 - \mathcal{R} \ll 1$), the resistance on the disturbance due to wave generation generally decreases as h increases from small values. For a more detailed discussion the reader is referred to [26].

Finally we consider the effect of z_0 in Fig. 6. As expected, there is a sharp variation in wave amplitudes around $z_0 \sim -h$ especially for smaller $\mathcal{R}$. As the location of the disturbance approaches the interface from below, a_n (especially $a_{\ell,n}$) increases markedly. As z_0 crosses $-h$, a_n drops abruptly proportionate to the abrupt drop in the density. As the disturbance approaches the free surface, $a_{\ell,n}$ decreases from its maximum value at $z_0 = -h$, while $a_{u,n}$ increases (eventually becoming unbounded as $z_0 \to 0$). The wave resistance on the disturbance as it crosses the interface consequently follows a similar qualitative trend.

4 Direct numerical simulation

For the general problem involving possibly multiple bodies and arbitrary time-dependence in the motions, the solution can be more generally and efficiently obtained by a direct numerical method. Here we present a highly efficient numerical scheme based on spectral expansion of potentials (Sect. 4.1). The numerical method is general for two- and three-dimensional problems and can be extended to account for nonlinear effects [27]. Here we focus on the linearized two-dimensional problem.

4.1 Formulation of the spectral method

Consider the linearized governing equations (2.1) with a point source located in either the upper or lower layer. For later convenience, we define $\varphi_u = \phi_u + \bar{\phi}_u$, $\varphi_\ell = \phi_\ell + \bar{\phi}_\ell$; where $\bar{\phi}_u$, $\bar{\phi}_\ell$ represent the potential of the point source in an unbounded homogeneous fluid, and, in the neighborhood of the interface, we define a new potential $\psi(x,z,t) \equiv \phi_\ell(x,z,t) - \mathcal{R}\phi_u(x,z,t)$. In terms of these quantities, and in the frame of reference moving with the disturbance, we can rewrite the kinematic and dynamic boundary conditions on the surface and interface in the forms:

$$\eta_{u,t} = U\eta_{u,x} + \phi_{u,z} + \bar{\phi}_{u,z}, \quad z = 0, \tag{4.56a}$$

$$\phi_{u,t} = U\phi_{u,x} - g\eta_u - \bar{\phi}_{u,t}, \quad z = 0, \tag{4.56b}$$

$$\eta_{\ell,t} = U\eta_{\ell,x} + \phi_{u,z} + \bar{\phi}_{u,z}, \quad z = -h_u, \tag{4.56c}$$

$$\psi_{,t} = U\psi_{,x} - g\eta_\ell(1-\mathcal{R}) - (\bar{\phi}_{\ell,t} - \mathcal{R}\bar{\phi}_{u,t}), \quad z = -h_u. \tag{4.56d}$$

In the numerical simulation, the equations of (4.56) are used as evolution equations for $\eta_u(x,t)$, $\phi_u(x,0,t)$, $\eta_\ell(x,t)$ and $\psi(x,-h_u,t)$, given the vertical surface velocity, $\phi_{u,z}(x,0,t)$, and the vertical interface velocities, $\phi_{u,z}(x,-h_u,t)$ and $\phi_{\ell,z}(x,-h_u,t)$, which are obtained from the solution of the boundary-value problem.

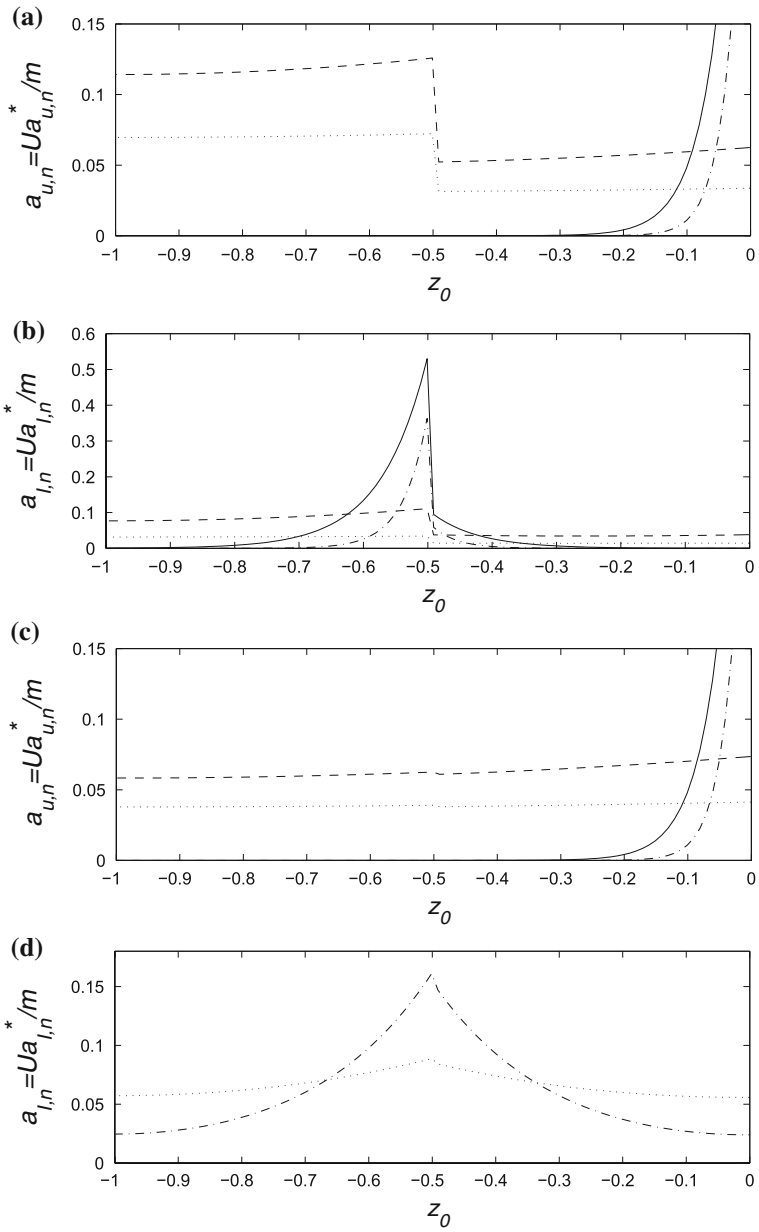

Fig. 6 Far-field wave amplitudes $a_{u,n}$, $a_{\ell,n}$, as functions of z_0 for $\mathcal{F}=0.03$, $\tau=0.1$, $h=0.5$, and, **a, b** $\mathcal{R}=0.2$; **c, d** $\mathcal{R}=0.95$. In Figs. **a, c** for $a_{u,n}$: $a_{u,1}$ ——; $a_{u,2}$ - - -; $a_{u,3}$ – · –; and $a_{u,4}$ · · ·. In Figs. **b, d** for $a_{\ell,n}$: $a_{\ell,5}$ ——; $a_{\ell,6}$ - - -; $a_{\ell,7}$ – · –; and $a_{\ell,8}$ · · ·

To find these velocities, we construct the solutions for ϕ_u and ϕ_ℓ in terms of Fourier basis functions:

$$\phi_u(x,z,t)=\sum_{n=-N}^{N-1}\left\{A_n(t)\frac{\cosh[k_n(z+h_u)]}{\cosh(k_nh_u)}+B_n(t)\frac{\sinh(k_nz)}{\cosh(k_nh_u)}\right\}\mathrm{e}^{\mathrm{i}k_nx}, \tag{4.57}$$

$$\phi_\ell(x,z,t)=\sum_{n=-N}^{N-1}C_n(t)\frac{\cosh[k_n(z+h_u+h_\ell)]}{\cosh(k_nh_\ell)}\,\mathrm{e}^{\mathrm{i}k_nx}, \tag{4.58}$$

where $k_n = 2\pi n/L$ with L being the length of the computational domain, and A_n, B_n, and C_n are the complex modal amplitudes. Clearly, ϕ_u and ϕ_ℓ in (4.57) and (4.58) are harmonic and satisfy the bottom boundary condition (2.1h). We note that, for sufficiently smooth ϕ_u and ϕ_ℓ, Eqs. (4.57) and (4.58) converge exponentially with increasing N. If initial conditions are given at time $t_0 = 0$:

$$\phi_u(x, 0, 0) = f_1(x), \quad \psi(x, -h_u, 0) = f_2(x), \tag{4.59}$$

then, by satisfying the remaining boundary conditions, the unknown amplitudes A_n, B_n, and C_n are obtained as

$$A_n = \tilde{f}_{1n}, \tag{4.60a}$$

$$B_n = \frac{\tilde{f}_{2n} + \mathcal{R}\tilde{f}_{1n}/\cosh(k_n h_u)}{\operatorname{cotanh} k_n h_\ell + \mathcal{R}\tanh k_n h_u}, \tag{4.60b}$$

$$C_n = \frac{B_n}{\tanh k_n h_\ell}\,. \tag{4.60c}$$

for $n = 0, \pm 1, \ldots, \pm N$. In (4.60), $\tilde{f}_{1n}$ and $\tilde{f}_{2n}$ are, respectively, the n-th Fourier modal amplitudes of $f_1(x)$ and $f_2(x)$. Once the boundary-value solution is obtained, the vertical velocities of the fluid on the free surface and interface are obtained from (4.57) and (4.58):

$$\phi_{u,z}(x, 0, t) = \sum_{n=-N}^{N} k_n \left[A_n(t)\tanh(k_n h_u) + B_n(t)\right] \mathrm{e}^{ik_n x}, \tag{4.61a}$$

$$\phi_{u,z}(x, -h_u, t) = \sum_{n=-N}^{N} k_n B_n(t) \mathrm{e}^{ik_n x}, \tag{4.61b}$$

$$\phi_{\ell,z}(x, -h_u, t) = \sum_{n=-N}^{N} k_n C_n(t)\tanh(k_n h_u) \mathrm{e}^{ik_n x}. \tag{4.61c}$$

To complete the evolution equations (4.56), if the source is located in the lower layer

$$\bar{\phi}_u = 0, \tag{4.62}$$

$$\bar{\phi}_\ell = \frac{m_0}{2\pi}(\log r_1 + \log r_2)\sin\omega_0 t, \tag{4.63}$$

where

$$r_1^2 = \sin^2\left(\frac{x - x_0}{2L/\pi}\right) + \sinh^2\left(\frac{z - z_0}{2L/\pi}\right), \tag{4.64}$$

$$r_2^2 = \sin^2\left(\frac{x - x_0}{2L/\pi}\right) + \sinh^2\left(\frac{z + 2h_u + 2h_\ell + z_0}{2L/\pi}\right), \tag{4.65}$$

and if the source is located in the upper layer:

$$\bar{\phi}_u = \frac{m_0}{2\pi}(\log r_1 + \log r_2)\sin\omega_0 t, \tag{4.66}$$

$$\bar{\phi}_\ell = 0, \tag{4.67}$$

where r_1 is the same as in (4.64), and

$$r_2^2 = \sin^2\left(\frac{x - x_0}{2L/\pi}\right) + \sinh^2\left(\frac{z + 2h_u + z_0}{2L/\pi}\right). \tag{4.68}$$

The time simulation of the initial-boundary-value problem consists of two main steps: (a) at each time t, given the surface and interface elevations $\eta_u(x, t)$ and $\eta_\ell(x, t)$, the surface potential and interfacial potentials $\phi_u(x, 0, t)$ and $\psi(x, -h_u, t) = \phi_\ell(x, -h_u, t) - \mathcal{R}\phi_u(x, -h_u, t)$; solve the boundary-value problems for ϕ_u and ϕ_ℓ and evaluate the surface and interfacial velocities $\phi_{u,z}(x, 0, t)$, $\phi_{u,z}(x, -h_u, t)$ and $\phi_{\ell,z}(x, -h_u, t)$; and (b) integrate the evolution equations (4.56) in time to obtain the new values of $\eta_u(x, t + \Delta t)$, $\eta_\ell(x, t + \Delta t)$, $\phi_u(x, 0, t + \Delta t)$ and

Table 1 Maximum error of the vertical interface velocity of a linearized wave matching the elevation profile of a Stokes wave in a two-layer fluid with $\epsilon = ka = 0.1$, $h_\ell / h_u = 1$, and $\mathcal{R} = 0.95$

	$N = 8$	$N = 16$	$N = 32$
Err	0.28×10^{-2}	0.65×10^{-5}	0.54×10^{-12}

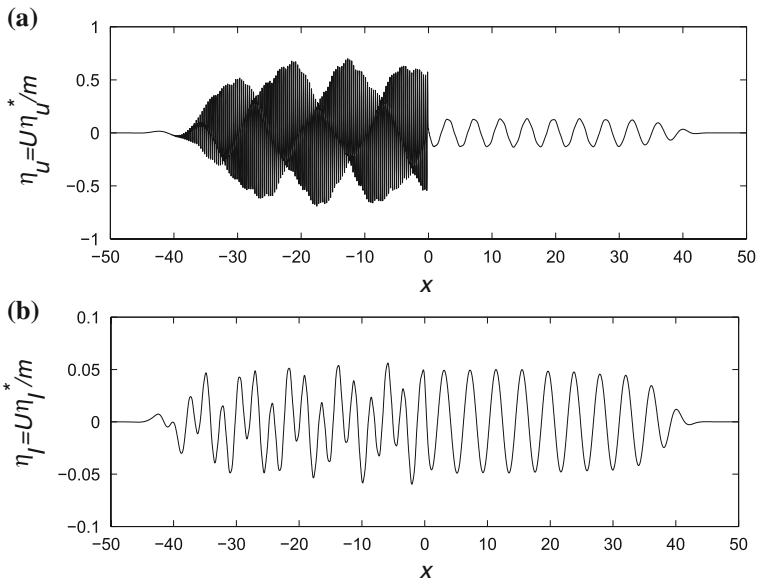

Fig. 7 Direct simulation results for **a** free surface, and **b** interfacial, wave elevations for $\mathcal{R} = 0.2$, $\mathcal{F} = 0.03$, $\tau = 0.16$, $z_0 = -0.02$ and $h = 0.5$. The numerical parameters are $N = 4{,}096$, $\Delta t = 0.03$, simulation time $T_f = 1{,}000$. In this and following figures flow is from right to left

$\psi(x, -h_u, t + \Delta t)$, where Δt is the time step. In the present work, a fourth-order Runge–Kutta integration scheme (with global truncation error $O((\Delta t/T)^4)$) is used. The two steps (a–b) are repeated starting from initial values.

To check the correctness and accuracy of our numerical scheme, we use an exact linearized solution for a wave in two fluid layers with a surface and interfacial wave elevations matching a Stokes wave solution [28]. Table 1 shows the exponential convergence in interface vertical velocity (compared to exact values) of the numerical spectral method with number of modes N.

4.2 Comparison with theory

The numerical scheme of course, provides an independent check of our analytic results in Sect. 3. For the numerical solution, we consider the problem of Sect. 3 in a frame of reference moving with the disturbance (at $x = 0$) and starting from quiescent initial conditions. The simulation is performed until steady state is reached in a finite portion $|x| < \bar{L}/2$ of the (periodic) computational domain whose length L is chosen to be sufficiently large so that the solution within $\bar{L}$ is unaffected. In practice, this can be achieved by applying a tapering filter for $|x| > L_f/2$ where $\bar{L} < L_f < L$. With this treatment, the simulation can proceed for a long time for a fixed $\bar{L}$ without increasing L.

Figure 7 shows the surface and interfacial elevation for a problem with $\mathcal{R} = 0.2$, $\mathcal{F} = 0.032$, $\tau = 0.16$, $z_0 = -0.02$, and $h = 0.5$ after a simulation time of $T_f = 1{,}000$. Note that the choice of z_0 is for the convenience of illustrating the *linear* solution. In fact in the direct simulation m_0 can be chosen small enough such that $a_{u,n} \ll |z_0|$. The computational parameters are: $L = 100$, $L_f = 75$, $N = 4{,}096$, and $\Delta t = 0.03$. With these parameters, the solution has reached steady state for $\bar{L} \approx 65$. For this set of parameters, $\tau_{\mathrm{cr},\ell} < \tau < \tau_{\mathrm{cr},u}$, $N_W = 6$ (four surface- and two

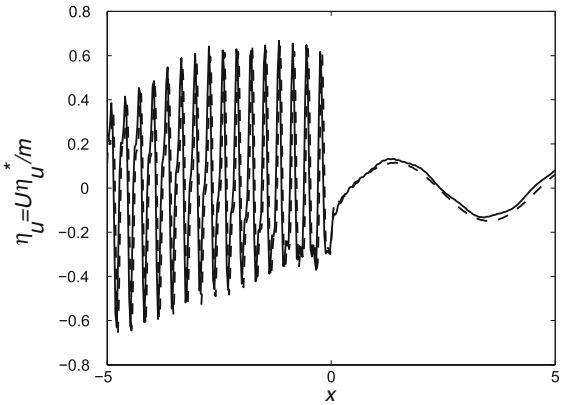

Fig. 8 Comparison of direct simulation (——) with theoretical prediction (- - -) in the near field of the moving disturbance for $\mathcal{R} = 0.2$, $\mathcal{F} = 0.03$, $\tau = 0.16$, $z_0 = -0.02$, $h = 0.5$. The numerical parameters are $N = 4{,}096$, $\Delta t = 0.03$, and $T_f = 750$

internal-mode waves) and no internal-mode wave propagate ahead of the disturbance (the interface wave elevation seen in front of the disturbance in Fig. 7b is associated with the k_2 forward traveling surface-mode wave). In Fig. 7, the magnitudes of $a_{u,n}$ are greater than those of $a_{\ell,n}$ because of the (somewhat arbitrary) choice of $z_0 = -0.02$. Note also that the visually seen sudden change of water surface amplitude in this figure is because of two orders of magnitude difference in the scale of x- and y-axes. With equal scales, water surface smoothly changes from one regime to the other.

Figure 8 compares the surface elevation computed by direct simulation with theoretical results of Sect. 3. For the analytical results, the principal value integrals in (3.32), (3.33) are evaluated using adaptive Lobatto quadrature. The comparison is almost within graphical accuracy, with the numerics capturing both the small k_2 wavenumber wave train ahead of the source and the modulated wave train (containing the small k_4 wavenumber and the larger k_1, k_3 wavenumber components) behind. To compare the predictions for the far-field amplitudes, the direct simulation results need to be processed for the constituent wave components. For a wavefield with N_c (expected) wave components, the amplitudes and phases at x are obtained by sampling the numerical result at say $N_p > 2N_c$ uniformly spaced points (Δx apart) centered at x, and then solving for the $2N_c$ unknown amplitude and phases by inverting an overdetermined linear algebraic system. The choice of Δx and N_p is important, and we generally require $k_{\max}\Delta x \ll 1$ and $N_p k_{\min}\Delta x \gtrsim O(1)$ to capture respectively the shortest and longest waves.

Figures 9 and 10 show such a set of results obtained from the numerics for the conditions: (a) $N_W = 8$: $\mathcal{F} = 0.032$, $\tau = 0.16$, $z_0 = -0.02$, $h = 1$ and $\mathcal{R} = 0.2$; and (b) $N_W = 4$: $\mathcal{F} = 0.128$, $\tau = 0.32$, $z_0 = -0.02$, $h = 1$ and $\mathcal{R} = 0.95$, respectively. The numerical results are compared to the far-field theoretical predictions (tabulated in Table 2). The simulation results and theoretical far-field amplitudes compare well for all the wave modes with the comparison somewhat better for the higher wavenumber components, since there are more of these waves sampled in the (finite) computational domain.

5 Conclusions

The linear problem of wave generation by a translating pulsating point source in a two-layer density-stratified fluid is studied analytically and numerically. The problem is motivated by the possibility of observing/characterizing the waves associated with ships and submarines in strong stratified waters that may be present, for example, in warm littoral zones.

From the dispersion relation, it is shown that $N_W = 4$, 6 or 8 waves can exist at the far-field of the disturbance depending on the parameters associated with the disturbance ($\mathcal{F}$, τ, z_0) and the ocean body ($\mathcal{R}$, h). The two- and three-dimensional Green functions are obtained analytically by solving the respective boundary-value problem. The Green functions give the entire wavefield and, of special interest, the far-field amplitudes associated with the N_W waves. These amplitudes depend qualitatively on the location of the disturbance (in the upper or lower fluid),

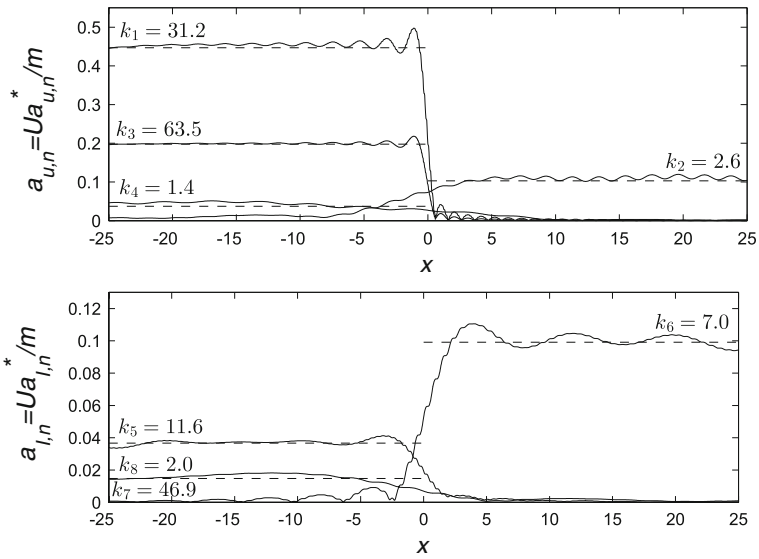

Fig. 9 Comparison of numerical simulations results (——) for the far-field wave amplitudes with theoretical values (- - -) for $\mathcal{R} = 0.2$, $\mathcal{F} = 0.032$, $\tau = 0.16$, $z_0 = -0.02$ and $h = 0.5$. The numerical parameters are $N = 4{,}096$, $\Delta t = 0.03$, and $T_f = 1{,}000$

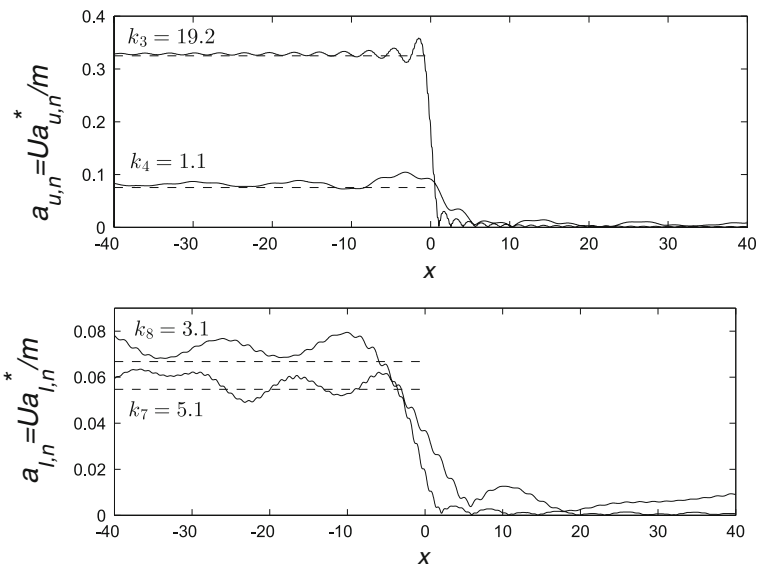

Fig. 10 Comparison of numerical simulations results (——) for the far-field wave amplitudes with theoretical values (- - -) for $\mathcal{R} = 0.95$, $\mathcal{F} = 0.128$, $\tau = 0.32$, $z_0 = -0.02$ and $h = 0.5$. The numerical parameters are $N = 4{,}096$, $\Delta t = 0.03$, and $T_f = 1{,}000$

the Froude number $\mathcal{F}$ and dimensionless frequency of pulsation τ of the disturbance, and the density ratio $\mathcal{R}$ and depth ratio h of the stratified layers. These dependencies are elucidated and discussed for $\mathcal{R}$=0.2 and 0.95, the latter being typical of real oceans.

For direct simulation, a spectral-based numerical scheme is developed. The numerical scheme is capable of simulating the general problem involving one or more bodies moving/oscillating arbitrarily with time. The numerical method, of course, also provides an independent check of the theoretical results, which we perform.

Table 2 Theoretical values for the dimensionless wave-number (k), frequency (ω), and surface- and interface-mode wave amplitudes a_u,a_ℓ for (a) $\mathcal{R}=0.2$, $h=0.5$, $\mathcal{F}=0.032$, $\tau=0.16$, $z_0=-0.02$; and (b) $\mathcal{R}=0.95$, $\mathcal{F}=0.128$, $h=0.5$, $\tau=0.32$, $z_0=-0.02$

	a				b			
n	k	ω	a_u	a_ℓ	k	ω	a_u	a_ℓ
1	31.2	5.00	0.447	0.000	–	–	–	–
2	2.6	1.34	0.130	0.027	–	–	–	–
3	63.5	7.13	0.198	0.000	19.2	3.92	0.325	0.001
4	1.4	−0.82	0.037	0.011	1.1	−0.72	0.075	0.035
5	11.6	2.49	0.004	0.037	–	–	–	–
6	7.0	1.89	0.041	0.099	–	–	–	–
7	46.9	5.00	0.000	0.000	5.1	0.31	0.001	0.055
8	2.0	−0.74	0.017	0.015	3.1	−0.22	0.001	0.067

The solution provided here together with Fourier superposition can be used to describe wave generation by a general variable strength source translating in a two-layer density-stratified fluid. The closed form solutions provided here can further be integrated with numerical schemes such as the Boundary Element Method to offer an efficient tool for a wave radiation/diffraction problem of general-shape finite bodies in layered fluids.

Acknowledgement This research is supported financially by grants from the Office of Naval Research.

Appendix: three-dimensional Green function

The three-dimensional Green function for a translating-oscillating source in a two-layer density-stratified fluid can be obtained similarly to the two-dimensional case. The analysis is in fact somewhat simpler because the fundamental singularity is no longer logarithmic. The final expressions for the three-dimensional Green function are given here.

For the source in the upper layer, we have

$$\phi_u = \frac{1}{r_4} + \frac{1}{r_5} + \int_{-\pi}^{\pi}\int_{0}^{\infty} (A\cosh kz + B\sinh kz)\, \mathrm{e}^{\mathrm{i}k(x\cos\theta + y\sin\theta)}\, \mathrm{d}k\, \mathrm{d}\theta, \tag{A.69}$$

$$\phi_\ell = \int_{-\pi}^{\pi}\int_{0}^{\infty} C\cosh k(z+1)\, \mathrm{e}^{\mathrm{i}k(x\cos\theta + y\sin\theta)}\, \mathrm{d}k\, \mathrm{d}\theta. \tag{A.70}$$

where $r_4^2 \equiv x^2+y^2+(z-z_0)^2$, $r_5^2 \equiv x^2+y^2+(z+2h+z_0)^2$. The coefficients A, B and C are obtained as

$$X = \frac{\alpha \hat{X}}{\lambda^4 - (\omega_s^2+\omega_i^2)\lambda^2 + \omega_s^2\omega_i^2}, \tag{A.71}$$

where X is either of A, B or C with

$$\hat{A} = -\beta\,\lambda^4 - \frac{\alpha k\,(-\mathcal{R}\,\mathrm{sl}\,\gamma + \mathrm{cl}\,\mathrm{cu}\,\beta + \mathcal{R}\,\mathrm{sl}\,\mathrm{su}\,\beta - \mathrm{sl}\,\beta\,\mathrm{cu} + \mathrm{sl}\,\mathcal{R}\beta\,\mathrm{cu})\,\lambda^2}{\mathrm{sl}\,\mathrm{su}\,\mathcal{R} + \mathrm{cu}\,\mathrm{cl}} - \frac{\alpha^2k^2\,\mathrm{sl}\,\mathrm{cu}\,\beta\;(-1+\mathcal{R})}{\mathrm{sl}\,\mathrm{su}\,\mathcal{R} + \mathrm{cu}\,\mathrm{cl}}, \tag{A.72}$$

$$\hat{B} = \frac{(\mathrm{sl}\,\mathrm{cu}\,\mathcal{R}\beta + \beta\,\mathrm{cl}\,\mathrm{su} - \mathcal{R}\,\mathrm{sl}\,\gamma)\,\lambda^4}{\mathrm{sl}\,\mathrm{su}\,\mathcal{R} + \mathrm{cu}\,\mathrm{cl}} + \frac{\alpha k\beta\;(\mathrm{sl}\,\mathrm{cu}\,\mathcal{R} + \mathrm{cl}\,\mathrm{su} - \mathrm{sl}\,\mathrm{su} + \mathrm{sl}\,\mathrm{su}\,\mathcal{R})\,\lambda^2}{\mathrm{sl}\,\mathrm{su}\,\mathcal{R} + \mathrm{cu}\,\mathrm{cl}} + \frac{\alpha^2k^2\beta\,\mathrm{sl}\,\mathrm{su}\;(-1+\mathcal{R})}{\mathrm{sl}\,\mathrm{su}\,\mathcal{R} + \mathrm{cu}\,\mathrm{cl}}, \tag{A.73}$$

$$\hat{C} = -\frac{\mathcal{R}\left(\mathrm{cu}^2\beta - \mathrm{cu}\,\gamma - \mathrm{su}^2\beta\right)\lambda^4}{\mathrm{cu}\,\mathrm{cl} + \mathrm{sl}\,\mathrm{su}\,\mathcal{R}} - \frac{\mathcal{R}\alpha k\left(-\mathrm{su}^2\beta + \mathrm{cu}^2\beta + \mathrm{su}\,\gamma\right)\lambda^2}{\mathrm{cu}\,\mathrm{cl} + \mathrm{sl}\,\mathrm{su}\,\mathcal{R}}, \tag{A.74}$$

where

$$\lambda = 1 - \mathcal{F}k\cos\theta/\tau, \quad \beta = \frac{\cosh k(z_0+h)}{\pi\ \exp(kh)}, \quad \gamma = \frac{\mathrm{e}^{-k(z_0+h)}}{\pi}\ .$$

For the source in the lower layer, we have

$$\phi_u = \int_{-\pi}^{\pi}\int_{0}^{\infty} (A\cosh kz + B\sinh kz)\,\mathrm{e}^{\mathrm{i}k(x\cos\theta + y\sin\theta)}\,\mathrm{d}k\,\mathrm{d}\theta, \tag{A.75}$$

$$\phi_\ell = \frac{1}{r_4} + \frac{1}{r_6} + \int_{-\pi}^{\pi}\int_{0}^{\infty} C\cosh k(z+1)\,\mathrm{e}^{\mathrm{i}k(x\cos\theta + y\sin\theta)}\,\mathrm{d}k\mathrm{d}\theta, \tag{A.76}$$

where $r_6^2 \equiv x^2 + y^2 + (2 + z + z_0)^2$, and

$$\hat{A} = -\frac{\alpha k\lambda^2\beta\ (\mathrm{sl} + \mathrm{cl})}{\mathrm{sl}\,\mathrm{su}\,\mathcal{R} + \mathrm{cl}\,\mathrm{cu}}, \quad \hat{B} = -\frac{\lambda^4\beta\ (\mathrm{sl} + \mathrm{cl})}{\mathrm{sl}\,\mathcal{R}\mathrm{su} + \mathrm{cl}\,\mathrm{cu}}, \tag{A.77}$$

$$\hat{C} = \frac{\beta\ (\mathrm{su}\,\mathcal{R} - \mathrm{cu})\,\lambda^4}{\mathrm{sl}\,\mathrm{su}\,\mathcal{R} + \mathrm{cl}\,\mathrm{cu}} - \frac{\beta\,\alpha k\,(\mathrm{cu} - \mathrm{su})\,\lambda^2}{\mathrm{sl}\,\mathrm{su}\,\mathcal{R} + \mathrm{cl}\,\mathrm{cu}} - \frac{\beta\,\alpha^2k^2\mathrm{su}\ (\mathcal{R} - 1)}{\mathrm{sl}\,\mathrm{su}\,\mathcal{R} + \mathrm{cl}\,\mathrm{cu}}, \tag{A.78}$$

where

$$\lambda = 1 - \mathcal{F}k\cos\theta/\tau, \quad \beta = \frac{\cosh k(z_0+1)}{\pi\ \mathrm{e}^{k(1-h)}}. \tag{A.79}$$

The limiting case of deep layers is instructive. For brevity, we consider only the case with N_W=8 ($\tau < \tau_{\mathrm{cr},i}$). For the source in the upper layer:

$$\begin{aligned}\phi_u = {} & \frac{1}{r_4} + \frac{1}{r_5} + \frac{2}{\pi}\int_{0}^{\frac{\pi}{2}}\int_{0}^{\infty} \frac{1}{\tau^4\cos^4\theta}(A\cosh kz + B\sinh kz)\sum_{q=1,2,5,6}\frac{a_q}{k-k_q}\,\mathrm{e}^{\mathrm{i}k(x\cos\theta + y\sin\theta)}\ \mathrm{d}k\mathrm{d}\theta \\ & + \frac{2}{\pi}\int_{\frac{\pi}{2}}^{\pi}\int_{0}^{\infty} \frac{1}{\tau^4\cos^4\theta}(A\cosh kz + B\sinh kz)\sum_{q=3,4,7,8}\frac{a_q}{k-k_q}\,\mathrm{e}^{\mathrm{i}k(x\cos\theta + y\sin\theta)}\,\mathrm{d}k\mathrm{d}\theta,\end{aligned} \tag{A.80}$$

$$\begin{aligned}\phi_\ell = {} & \frac{2}{\pi}\int_{0}^{\frac{\pi}{2}}\int_{0}^{\infty} \frac{1}{\tau^4\cos^4\theta}\,C\cosh k(z+1)\sum_{q=1,2,5,6}\frac{a_q}{k-k_q}\,\mathrm{e}^{\mathrm{i}k(x\cos\theta + y\sin\theta)}\,\mathrm{d}k\mathrm{d}\theta \\ & + \frac{2}{\pi}\int_{\frac{\pi}{2}}^{\pi}\int_{0}^{\infty} \frac{1}{\tau^4\cos^4\theta}\,C\cosh k(z+1)\sum_{q=3,4,7,8}\frac{a_q}{k-k_q}\,\mathrm{e}^{\mathrm{i}k(x\cos\theta + y\sin\theta)}\,\mathrm{d}k\mathrm{d}\theta,\end{aligned} \tag{A.81}$$

where

$$a_q = \prod_{j=\{1,2,5,6\}-q}\frac{1}{\alpha^3}\cdot\frac{1}{k_q - k_j} \quad \text{for } q = 1, 2, 5, 6, \tag{A.82}$$

$$a_q = \prod_{j=\{3,4,7,8\}-q}\frac{1}{\alpha^3}\cdot\frac{1}{k_q - k_j} \quad \text{for } q = 3, 4, 7, 8. \tag{A.83}$$

For the source in the lower layer, the expressions for the deep layers Green function are:

$$\phi_u = \frac{2}{\pi}\int_0^{\frac{\pi}{2}}\int_0^{\infty} \frac{1}{\tau^4\cos^4\theta}(A\cosh kz + B\sinh kz)\sum_{q=1,2,5,6}\frac{a_q}{k-k_q}\,\mathrm{e}^{\mathrm{i}k(x\cos\theta+y\sin\theta)}\,\mathrm{d}k\,\mathrm{d}\theta$$
$$+\frac{2}{\pi}\int_{\frac{\pi}{2}}^{\pi}\int_0^{\infty} \frac{1}{\tau^4\cos^4\theta}(A\cosh kz + B\sinh kz)\sum_{q=3,4,7,8}\frac{a_q}{k-k_q}\,\mathrm{e}^{\mathrm{i}k(x\cos\theta+y\sin\theta)}\,\mathrm{d}k\,\mathrm{d}\theta, \tag{A.84}$$

$$\phi_\ell = \frac{1}{r_4}+\frac{1}{r_6}+\frac{2}{\pi}\int_0^{\frac{\pi}{2}}\int_0^{\infty} \frac{1}{\tau^4\cos^4\theta}\,C\cosh k(z+1)\sum_{q=1,2,5,6}\frac{a_q}{k-k_q}\,\mathrm{e}^{\mathrm{i}k(x\cos\theta+y\sin\theta)}\,\mathrm{d}k\,\mathrm{d}\theta,$$
$$+\frac{2}{\pi}\int_{\frac{\pi}{2}}^{\pi}\int_0^{\infty} \frac{1}{\tau^4\cos^4\theta}\,C\cosh k(z+1)\sum_{q=3,4,7,8}\frac{a_q}{k-k_q}\,\mathrm{e}^{\mathrm{i}k(x\cos\theta+y\sin\theta)}\,\mathrm{d}k\,\mathrm{d}\theta\ . \tag{A.85}$$

While the two-dimensional Green function predicts waves with a constant amplitude at infinity, similar to the homogeneous fluid case, amplitudes of waves of a three-dimensional source decay with the distance from the source. Since the wave-number vector of the generated waves is a function of the polar angle (θ) in the horizontal plane, the surface/interfacial-wave pattern of a three-dimensional translating/oscillating source is much more complex than those in two dimensions [8].

References

1. Wei G, Lu D, Dai S (2005) Waves induced by a submerged moving dipole in a two-layer fluid of finite depth. Acta Mech Sin 21(1):24–31
2. Avital E, Miloh T (1999) On an inverse problem of ship-induced internal waves. Ocean Eng 26(2):99–110
3. Avital E, Miloh T (1994) On the determination of density profiles in stratified seas from kinematical patterns of ship-induced internal waves. J Ship Res 38(4):308–318
4. Haskind MD (1954) On the motion with waves of heavy fluid (in Russian). Prikl Mat Mekh 18:15–26
5. Wehausen JV, Laitone EV (1960) Surface waves. In: Handbuch der Physik, vol 9, Part 3. Springer-Verlag, Berlin, pp 446–778
6. Akylas TR (1984a) On the excitation of long nonlinear water waves by a moving pressure distribution. J Fluid Mech 141:455–466
7. Akylas TR (1984b) On the excitation of nonlinear water waves by a moving pressure distribution oscillating at resonant frequency. Phys Fluids 27(12):2803–2807
8. Liu Y, Yue DKP (1993) On the solution near the critical frequency for an oscillating and translating body in or near a free surface. J Fluid Mech 254:251–266
9. Palm E, Grue J (1999) On the wave field due to a moving body performing oscillations in the vicinity of the critical frequency. J Eng Math 35(1-2):219–232
10. Baines PG (1997) Topographic effects in stratified flows. In: Batchelor GK, Freud LB (eds) Cambridge monographs on mechanics. Cambridge University Press, Cambridge
11. Voitsenya VS (1958) The two dimensional problem of the oscillations of a body under the surface of separation of two fluids (Russian). Prikladnaia matematika i mekhanika [Appl Math Mech] 22(8):789–803
12. Hudimac AA (1961) Ship waves in a stratified ocean. J Fluid Mech 11:229–243
13. Crapper GD (1967) Ship waves in a stratified ocean. J Fluid Mech 29:667–672
14. Sharman RD, Wurtele MG (1983) Ship waves and lee waves. J Atmos Sci 40(2):396–427
15. Yeung RW, Nguyen TC (1999) Waves generated by a moving source in a two-layer ocean of finite depth. J Eng Math 35(1–2):85–107
16. Lu DQ, Chwang AT (2005) Interfacial waves due to a singularity in a system of two semi-infinite fluids. Phys Fluids 17(10):102107–102109
17. Dommermuth DG, Yue DKP (1987) A higher-order spectral method for the study of nonlinear gravity waves. J Fluid Mech 184:267–288
18. Lamb H (1932) Hydrodynamics. Dover, New York
19. Ball F (1964) Energy transfer between external and internal gravity waves. J Fluid Mech 19:465–478
20. Alam M-R, Liu Y, Yue DK (2009) Bragg resonance of waves in a two-layer fluid propagating over bottom ripples. Part I: perturbation analysis. J Fluid Mech 624:191–224

21. Faltinsen O (1993) Sea loads on ships and offshore structures. Cambridge University Press, Cambridge
22. McCauley JL Jr (1979) Phase space quantisation of interacting vortices in two dimensions. J Phys A 12(11):1999–2013
23. Thorne RC (1953) Multipole expansions in the theory of surface waves. Proc Cambridge Philos Soc 49:707–716
24. Debnath L (1971) On transient development of surface waves due to two dimensional sources. Acta Mech 11:185–202
25. Shen H, He Y (2005) Study internal waves in north west of south China sea by satellite images. In: Geoscience and remote sensing symposium, proceedings 2005, IEEE International 4, IGARSS'05
26. Alam M-R (2008) Interaction of waves in a two-layer density stratified fluid. PhD thesis, Massachusetts Institute of Technology, Cambridge, MA, USA
27. Tsai W-T, Yue DKP (1996) Computation of nonlinear free-surface flows. Annu Rev Fluid Mech 28:249–278
28. Alam M-R, Liu Y, Yue DK (2009) Bragg resonance of waves in a two-layer fluid propagating over bottom ripples. Part II: numerical simulation. J Fluid Mech 624:225–253